PHYSICAL REVIEW B **78**, 180101(R) (2008)

Shear stresses in shock-compressed diamond from density functional theory

Ivan I. Oleynik,[1] Aaron C. Landerville,[1] Sergey V. Zybin,[2] Mark L. Elert,[3] and Carter T. White[4]
[1]*Department of Physics, University of South Florida, Tampa, Florida 33620, USA*
[2]*Materials and Process Simulation Center, Beckman Institute, California Institute of Technology, Pasadena, California 91125, USA*
[3]*U.S. Naval Academy, Annapolis, Maryland 21402, USA*
[4]*Naval Research Laboratory, Washington, DC 20375, USA*
(Received 9 September 2008; published 20 November 2008)

We report density functional theory (DFT) results for the shear stresses of uniaxially compressed diamond under conditions corresponding to strong shock wave compression. A nonmonotonic dependence of shear stresses on uniaxial strain was discovered in all three low-index crystallographic directions: ⟨100⟩, ⟨110⟩, and ⟨111⟩. For ⟨100⟩ compression the shear stress even becomes negative in the region near the minimum of the shear stress-strain curve. The DFT results suggest that anomalous elastic regime observed in recent molecular dynamics shock simulations is a real phenomenon caused by a significant delay or even freezing of the plastic response.

DOI: 10.1103/PhysRevB.78.180101 PACS number(s): 62.50.Ef

Diamond is a unique material with many exceptional physical properties.[1] The diamond crystal is very resistant to shear deformation because of a strong angular dependence in the interatomic interactions. In fact, it is one of a handful of materials where the shear moduli, $C'=(C_{11}-C_{12})/2=4.76$ Mbar and $C_{44}=5.77$ Mbar, are larger than the bulk modulus, $B=(C_{11}+2C_{12})/3=4.43$ Mbar, which is the highest of all elemental solids. The unusual hardness of diamond is a direct consequence of its shear stiffness; a property successfully exploited in the diamond-anvil cells used as the primary tool for generating ultrahigh pressures in the laboratory.[2,3]

One of the attractive methods in probing extreme mechanical properties of diamond is to subject it to shock compression.[4] Experimental results for mechanical properties of shock-compressed diamond are only beginning to emerge.[5–9] Recently, we employed the hydrocarbon reactive empirical bond-order (REBO) potential[10,11] to perform large-scale molecular dynamics (MD) simulations of shock wave propagation in diamond along the ⟨100⟩, ⟨110⟩, and ⟨111⟩ directions.[12] These simulations are aimed at stimulating future experimental efforts and providing insight into the orientational dependence of shock-induced chemistry.[13,14] With increasing shock wave intensity, we observed four different regimes of materials response: a pure elastic regime, a shock wave splitting into elastic and plastic waves, an anomalous elastic regime, and an overdriven plastic wave with activated carbon chemistry.[12,14]

The anomalous elastic response in shock-compressed diamond is characterized by the absence of plastic deformations, including point and extended defects in a highly compressed diamond lattice as depicted in Fig. 1. The shock wave intensities corresponding to the anomalous elastic regime lie between those resulting in plastic deformation and those that initiate carbon chemistry in highly compressed diamond. We were able to relate this regime to a nonmonotonic behavior of shear stress as a function of uniaxial compression.[14] However this correspondence was made using a hydrocarbon REBO potential, which is known to provide a good description of mechanical properties of diamond at equilibrium but has not yet been tested at very high pressures and stresses. Therefore, it is unclear whether the anomalous elastic regime found in the MD simulations is a real phenomenon or just an artifact of this potential.

Herein, we report results of a density functional theory (DFT) investigation of diamond under uniaxial compression at zero temperature in the ⟨100⟩, ⟨110⟩, and ⟨111⟩ directions in the strain interval $0\leq\varepsilon\leq 0.7$. We found that the nonmonotonic behavior of the shear stress under uniaxial compression originally observed in calculations using the REBO potential is also seen in the DFT calculations, indicating that this is a real response. The results, however, show that either the hydrocarbon REBO potential be modified or new potentials be introduced to better reproduce the high-pressure DFT results.

The unit cells used in these studies are shown in Fig. 2. Different strains were imposed by varying the c axis of a particular cell. For each value of c, the lateral dimensions of the cell were held fixed and all the atomic coordinates were relaxed to have zero net forces on the atoms. The starting

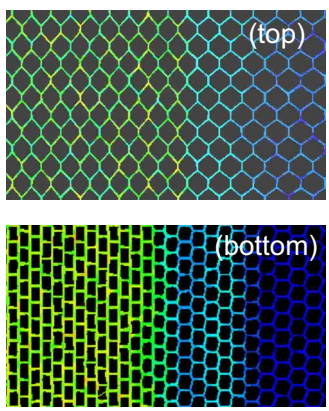

FIG. 1. (Color online) Snapshots of the shock front in the anomalous elastic region for a ⟨110⟩ shock wave (top) resulting in a compression ratio of 0.795, and a ⟨111⟩ shock wave (bottom) resulting in a compression ratio of 0.715. Atoms are colored according to potential energy [blue (dark gray) corresponds to low, and yellow (light gray) to high energy]. For clarity only the top few layers are shown and small cutouts of the full MD simulations are depicted.

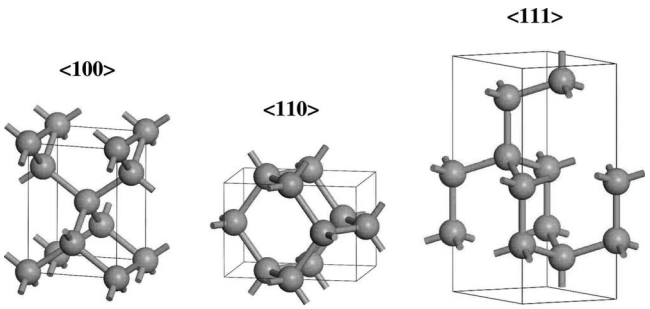

FIG. 2. Unit cells used in calculating the effects of uniaxial compression along the ⟨100⟩, ⟨110⟩, and ⟨111⟩ directions.

atomic coordinates were obtained from the atomic coordinates of the previously relaxed structure with larger c. Uniaxial compression at fixed lateral dimensions corresponds to the conditions of shock wave experiments at sufficiently large shock wave intensities. The time scale associated with the initial process of shock wave compression is on the order of picoseconds or less (the thickness of the shock wave front is of the order of several lattice constants and the shock wave velocity is several km/s). Therefore, the lattice rapidly transforms at the shock wave front to a uniaxially compressed state.

This condition of pure uniaxial compression of shocked diamond differs from conditions resulting from indentation or diamond-anvil cell compression where the mechanical loading is comparatively slow so that the stresses in the lateral dimensions are able to relax (at least partially) through lateral expansion of the lattice. Hence, our initial conditions differ from those used in several other DFT calculations of shear deformations,[15,16] where the conditions of diamond-anvil cell experiments (specific combination of uniaxial and hydrostatic strains[15,16]) or the conditions of nanoindentation and diamond cleavage experiments (full relief of stresses in lateral dimensions[17–19]) were used. Calculations of pure uniaxial compression of diamond similar to our calculations were performed by Nielsen.[20] However, his study did not reach the high degree of compression where the shear stresses exhibit nonmonotonic behavior.

Our DFT calculations were performed using the Vienna *ab initio* simulation package (VASP) (Refs. 21 and 22) within a generalized gradient approximation (GGA) for the electronic exchange and correlation (PBE GGA functional was used).[23] The projector-augmented wave (PAW) potential and a large plane-wave cut-off energy of 700 eV were used. Recent work has demonstrated that even at high compression the pseudopotential and PAW methods give almost indistinguishable results from those obtained by all-electron

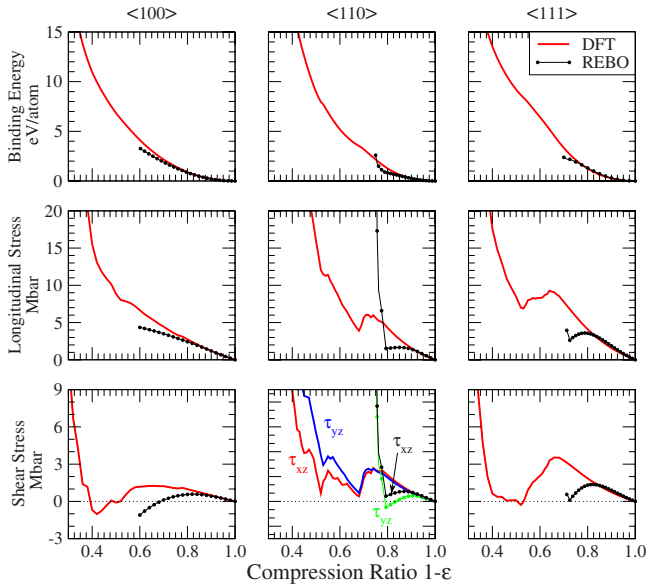

FIG. 3. (Color online) Binding energy (top), longitudinal stress (middle), and shear stress (bottom) for uniaxial compression along ⟨100⟩, ⟨110⟩, and ⟨111⟩ directions.

methods.[24] A possible appearance of metallic phases in the course of uniaxial compression requires dense sampling of the k-space Brillouin zone; thus the k-point spacing was 0.05 $Å^{-1}$. The particular values of the energy cutoff and k-space sampling density were chosen to achieve an accuracy in the calculated stresses that is better than 0.1 GPA, and in the calculated energies that is better than 10^{-3} eV per atom. The calculated values of lattice and elastic constants are in good agreement with experiment, as shown in Table I.

We compare DFT to REBO results for the binding energy per atom as a function of physical strain at the top of Fig. 3. The DFT and REBO binding energies are in good agreement for strains up to 0.25 in the ⟨100⟩ and ⟨111⟩ directions, and 0.15 in the ⟨110⟩ direction. The REBO results plotted in Fig. 3 cover a smaller strain range than the DFT results because at very large strains we faced problems due to the finite cut-off radius of interatomic interactions. Discontinuities in the slope of the binding energy for the ⟨110⟩ and ⟨111⟩ directions are the signatures of polymorphic phase transitions occurring at large compression ratios. For example, at $1-\varepsilon \simeq 0.6$, the ⟨111⟩ compressed diamond crystal structure transforms into the structure with atomic arrangements close to those in a simple hexagonal lattice.

The longitudinal stress, σ_{zz}, as a function of uniaxial strain is shown in Fig. 3 (middle). The good agreement between the DFT and REBO data is now observed in a nar-

TABLE I. DFT and REBO bulk properties (lattice parameter in angstrom and elastic constants in MBar) of diamond as compared with experiment.

Method	a	C_{11}	C_{12}	C_{44}	B	C'
DFT	3.530	11.0	1.19	5.86	4.42	4.90
REBO	3.556	10.7	1.00	6.8	4.23	4.85
Expt.	3.567	10.7	1.25	5.77	4.43	4.76

rower interval of uniaxial strain: $0 \leq \varepsilon \leq 0.15$ for the $\langle 100 \rangle$ and $\langle 111 \rangle$ directions, and $0 \leq \varepsilon \leq 0.1$ for the $\langle 110 \rangle$ direction, which reflects the fact that the stresses are first-order derivatives of energy per unit volume on strain. The longitudinal stress shows monotonic behavior as a function of strain in the $\langle 100 \rangle$ direction but exhibits a local maximum and minimum in the $\langle 110 \rangle$ and $\langle 111 \rangle$ directions. Results from DFT and REBO calculations show qualitatively similar behavior but the positions of the extrema and the values of the stresses are different. These local extrema are the primary sources of the nonmonotonic behavior of shear stresses for the $\langle 110 \rangle$ and $\langle 111 \rangle$ directions shown in Fig. 3.

In contrast, the nonmonotonic behavior of shear stress in the $\langle 100 \rangle$ direction shown at the bottom of Fig. 3 is due to the change of slope of both lateral $\sigma_{xx(yy)}$ and longitudinal σ_{zz} stress profiles. Although $\sigma_{xx(yy)}$ are monotonic with $\sigma_{zz} > \sigma_{xx(yy)}$ at small strains, they first approach and then become larger than σ_{zz} in the intermediate range of ε's. Upon further increase in the strain, the slope of σ_{zz} begins to increase resulting in the next crossover, $\sigma_{zz} = \sigma_{xx(yy)}$, with σ_{zz} again larger than $\sigma_{xx(yy)}$ at very large compressions.

Uniaxial compression in the z direction creates the maximum shear stresses $\tau_{xz} = (1/2)(\tau_{zz} - \tau_{xx})$ and $\tau_{yz} = (1/2)(\tau_{zz} - \tau_{yy})$ that are directed at 45° to the direction of the compression. It is the shear stress that drives plastic deformations when exceeding a threshold value. The DFT and REBO shear stress profiles are shown in Fig. 3 (bottom). The shear stresses τ_{xz} and τ_{yz} are equal for the $\langle 100 \rangle$ and $\langle 111 \rangle$ directions because of the symmetry of the diamond lattice. Therefore, only one of them is shown in the left and right panels of Fig. 3 (bottom). Both results from the REBO potential and DFT exhibit nonmonotonic behavior of the shear stresses for all three crystallographic directions. The DFT shear stresses initially increase, reach a maximum, decrease, reach a minimum, and increase again at very large compressions. The DFT maximum and subsequent minimum are at compression ratios 0.65 and 0.425 for the $\langle 100 \rangle$ direction, 0.75 and 0.675 (τ_{xz}), 0.725 and 0.675 (τ_{yz}) for the $\langle 110 \rangle$ direction, and 0.675 and 0.525 for the $\langle 111 \rangle$ direction [see Fig. 3 (bottom)]. The REBO results show similar behavior but, due to problems with the finite cut-off radius, the shear profiles are limited to smaller strains.

Both DFT and the REBO potential predict that the shear stresses approach small values for both the $\langle 110 \rangle$ and $\langle 111 \rangle$ directions which were studied in the MD shock simulations.[12] This causes important changes in the mechanical properties of shock-compressed diamond. We observed no plastic deformations in our MD simulations in just this range of uniaxial compressions.[12] In contrast, in the regime of smaller compressions, plastic deformations occurred by displacement of the atoms in the direction of the maximum shear stress. This causes stress relief in the compressed lattice. The same picture was observed at higher uniaxial compressions when the shear stress again becomes appreciable. Because the shear stress is the driving force for the lateral movement, the slipping of the crystal planes, and the creation of both point and extended defects, there will be some range of uniaxial compressions where these processes are inhibited or even frozen due to small values of shear stress near the minima of the shear profiles in Fig. 3 (bottom). This anomalous elastic state might ultimately transform to a plastic state behind the shock front with the transformation initiated by random thermal movement in the shock-heated crystal. However, we have not observed this instability in our MD simulations, suggesting that this anomalous elastic state, even if unstable, could persist for long enough times to be experimentally observable.

In spite of quantitative problems with the REBO potential at large compressions, the DFT results indicate that the anomalous elastic regime seen in MD simulations using this potential is a real phenomenon that should be observable in sufficiently resolved experiments. These phenomena may also occur in several other materials that exhibit nonmonotonic shear stress-strain relationships.[25] Our results also show that further work is required to develop robust and transferable interatomic potentials for a quantitative description of strong shock waves in condensed matter even for a relatively simple system such as diamond. Moreover, our results provide benchmarks for testing other classical carbon potentials at conditions appropriate for strong shock wave simulations.

This work was supported by the U.S. Office of Naval Research (ONR) both directly and through the Naval Research Laboratory (NRL). The computations were performed using NSF Teragrid computational facilities (Grant No. TG-DMR070018N).

[1] *Properties of Natural and Synthetic Diamond*, edited by J. E. Field (Academic Press, New York, 1992).
[2] H. K. Mao and R. J. Hemley, Nature (London) **351**, 721 (1991).
[3] A. L. Ruoff, H. Luo, and Y. K. Vohra, J. Appl. Phys. **69**, 6413 (1991).
[4] See, for example, *High Pressure Shock Compression of Solids*, edited by L. Davison and M. Shahinpoor (Springer, New York, 1998), Vols. I–III.
[5] J. B. Donnet, E. Fousson, T. K. Wang, M. Samirant, C. Baras, and M. Pontier Johnson, Diamond Relat. Mater. **9**, 887 (2000).
[6] G. R. Willmott, W. G. Proud, and J. E. Field, J. Phys. IV France **110**, 833 (2003).
[7] D. K. Bradley, J. H. Eggert, D. G. Hicks, P. M. Celliers, S. J. Moon, R. C. Cauble, and G. W. Collins, Phys. Rev. Lett. **93**, 195506 (2004).
[8] H. Nagao, K. G. Nakamura, K. Kondo, N. Ozaki, K. Takamatsu, T. Ono, T. Shiota, D. Ichinose, K. A. Tanaka, K. Wakabayashi, K. Okada, and M. Yoshida, Phys. Plasmas **13**, 052705 (2006).
[9] S. Brygoo, E. Henry, P. Loubeyre, J. Eggert, M. Koenig, B. Loupias, A. Benuzzi-Mounaix, and M. R. Le Gloahec, Nature Mater. **6**, 274 (2007).
[10] D. W. Brenner, O. A. Shenderova, J. A. Harrison, S. J. Stuart, B. Ni, and S. B. Sinnott, J. Phys.: Condens. Matter **14**, 783 (2002).
[11] D. W. Brenner, Phys. Rev. B **42**, 9458 (1990).

[12] K. McLaughlin, I. I. Oleynik, S. V. Zybin, M. L. Elert, and C. T. White, in *Shock Compression of Condensed Matter–2007*, edited by M. Elert *et al.*, AIP Conf. Proc. No. 955 (AIP, New York, 2007), p. 321.
[13] S. V. Zybin, M. L. Elert, and C. T. White, Phys. Rev. B **66**, 220102(R) (2002).
[14] S. V. Zybin, I. I. Oleynik, M. L. Elert, and C. T. White, in *Synthesis, Characterization and Properties of Energetic/ Reactive Nanomaterials*, MRS Symposia Proceedings No. 800 (Materials Research Society, Pittsburgh, 2003), p. AA7.7.
[15] P. E. van Camp, V. E. van Doren, and J. T. Devreese, Solid State Commun. **84**, 731 (1992).
[16] J. J. Zhao, S. Scandolo, J. Kohanoff, G. L. Chiarotti, and E. Tosatti, Appl. Phys. Lett. **75**, 487 (1999).
[17] R. H. Telling, C. J. Pickard, M. C. Payne, and J. E. Field, Phys. Rev. Lett. **84**, 5160 (2000).
[18] H. Chacham and L. Kleinman, Phys. Rev. Lett. **85**, 4904 (2000).
[19] D. Roundy and M. L. Cohen, Phys. Rev. B **64**, 212103 (2001).
[20] O. H. Nielsen, Phys. Rev. B **34**, 5808 (1986).
[21] G. Kresse and J. Furthmuller, Phys. Rev. B **54**, 11169 (1996).
[22] G. Kresse and J. Furthmuller, Comput. Mater. Sci. **6**, 15 (1996).
[23] J. P. Perdew, K. Burke, and M. Ernzerhof, Phys. Rev. Lett. **77**, 3865 (1996).
[24] K. Kunc, I. Loa, and K. Syassen, Phys. Rev. B **68**, 094107 (2003).
[25] D. C. Swift and G. J. Ackland, Appl. Phys. Lett. **83**, 1151 (2003).